Supplementary Information

Anion doping and interfacial effects in B-Ni_5P_4/Ni_2P promoting urea-assisted hydrogen production in alkaline media

*Mingming Sun[a,1], Huichao Wang[b,1], Hongjing Wu[b], Yuquan Yang[b], Jiajia Liu[b], Riyu Cong[b], Zhengwenda Liang[c], Zhongning Huang[e,] *, Jinlong Zheng[c, d,] **

[a] Basic Experimental Center for Natural Science, University of Science and Technology Beijing, Beijing, 100083, China

[b] School of Mathematics and Physics, University of Science and Technology Beijing, Beijing, 100083, China

[c] Beijing Advanced Innovation Center for Materials Genome Engineering, University of Science and Technology Beijing, Beijing, 100083, China

[d] Shunde Innovation School, University of Science and Technology Beijing, Foshan, 528399, China

[e] School of Chemistry, Beihang University, Beijing, 100191, China

[1] These authors contributed equally to this work.

Experimental section

1 Materials and chemicals

Nickel foam, Na_2SO_4, $NaBH_4$, KOH. The above experimental drugs were purchased from Beijing Tong Guang Fine Chemical Company. $Ni(NO_3)_2 \cdot 6H_2O$, NaH_2PO_2, urea and ethanol were purchased from Aladdin. Co. Ltd. Samples were washed with ultra-pure water during material preparation.

2 Material preparations

2.1 Preparation of the $Ni(SO_4)_{0.3}OH_{1.4}$ precursor on Ni foam

First, the foam nickel was cut into 2.2 cm x 2.2 cm size, soaked in a well-configured dilute hydrochloric acid solution for 5 minutes to remove impurities on the surface of the foam nickel, washed with ethanol and deionized water successively, and dried for further experiment. Then, 0.29 g $Ni(NO_3)_2 \cdot 6H_2O$ and 0.142 g Na_2SO_4 were dissolved into 20 ml ultrapure water, and the uniform solution was transferred to a 50 mL Teflon autoclave after ultrasonic treatment for 10 minutes. The mixed solution was sealed in a 160 °C oven and heated for 6-8 h, then washed several times with ultra-pure water and ethanol and dried.

2.2 Preparation of Ni_5P_4/Ni_2P on Ni foam

Ni_5P_4/Ni_2P@NF was obtained by low temperature phosphating in a tube furnace. First, the $Ni(SO_4)_{0.3}OH_{1.4}$ precursor (2.2 cm ×2.2 cm) and NaH_2PO_2 (400 mg) were placed in two clean porcelain boats and the phosphorus source was located upstream of the tube furnace. And calcined in tube furnace at 350 ℃ for 2 h with the heating rate of 1 ℃/min. During the whole phosphating process, nitrogen was injected as a protective gas (30 sccm). After finishing and cooling, Ni_5P_4/Ni_2P@NF was collected for later use. Then the experimental operation was repeated and the phosphating temperature was adjusted to 300 °C and 400 °C respectively to synthesize Ni_2P and Ni_5P_4.

2.3 Preparation of B-doped Ni_5P_4/Ni_2P on Ni foam

Firstly, 10 mg of $NaBH_4$ was fully dissolved in 30 mL deionized water to obtain $NaBH_4$ aqueous solution, and then Ni_5P_4/Ni_2P@NF (2.2 cm × 2.2 cm) was slowly immersed

in the $NaBH_4$ aqueous solution for 30 minutes to complete the doping of B ions. After soaking, it was repeatedly rinsed with deionized water and ethanol for 3 times, and dried in oven at 40 ℃ for 10 h.

3 Fabrication of Pt/C and RuO_2 electrodes

10 mg Pt/C powder was fused with 330 μL ultra-pure water, 330 μL anhydrous ethanol, 330 μL opropyl alcohol, and 10 μL Nafion solution, and a uniform solution was obtained 30 minutes after ultrasound. The 200 μL Pt/C electrode was then coated on a 3 mm diameter glassy carbon electrode (GC) and finally dried in a 45 °C vacuum. The RuO_2 electrode was also prepared in the same way.

4 Physical and Chemical Characterization

The diffraction pattern was obtained by X-ray diffraction through Rigaku D/max 2550 diffractometer to determine the composition of the sample. The radiation source was Cu Ka and its wavelength was 1.5418 Å. Scanning electron microscopy (SEM) images are scanned by the JEOL JSM-6701F instrument with an accelerated voltage of 15.0 KV. At the same time, transmission electron microscopy (TEM) and high-resolution transmission electron microscopy (HRTEM) were observed on the JEOL-2200FS instrument with an operating voltage of 150 KV. At 200 kV, the samples were characterized by high Angle toroidal dark field scanning TEM (HAADF-TEM) and energy dispersive spectroscopy (EDS) by JOEL JEM-2200FS. X-ray photoelectron spectroscopy (XPS) was obtained by using Al Kα as X-ray source and PHI 5000 Versaprobe III.

5 Electrochemical measurements

All electrochemical tests are performed using a typical three-electrode system through electrochemical workstation (CHI760E, CH Instruments Inc., Shanghai). Graphite rods are used as the reverse electrode, Hg/HgO was used as the reference electrode, and the sample was prepared as the working electrode. 1 M KOH (pH = 14) aqueous solution at room temperature was used as the electrolyte to evaluate the HER performance of the sample. The UOR properties of the samples were evaluated at room temperature by adding urea into 1 M KOH aqueous solution as electrolyte. All potentials are converted to reversible hydrogen electrode (RHE) by the following formula:

$E_{RHE}=E_{Hg/HgO} + 0.098 + 0.0591 \times pH$ (Alkaline solution)

All current densities are calculated according to the geometric surface area of the working electrode (~0.025 cm^{-2}). The linear sweep voltammetry curves of HER performance were recorded in different electrolytes at a scanning rate of 1 mV/s. EIS measurements are performed at the open-circuit potential with a frequency range from 0.1 to 100,000 Hz. And CV curves are obtained at different sweep rates (10, 20, 30, 40, 50, 60, 70, and 80 mV/s) in the non-Faraday potential range to determine the double-layer capacitance (C_{dl}). The electrochemically active surface area (ECSA) was calculated as follows: $ECSA = C_{dl}/C_s$

Where C_s is the specific capacitance value (~40 μF cm^{-2}) of the sample with smooth surface under the same conditions. The aqueous solution of 1 M KOH containing 0.1 M ~ 0.5 M urea at room temperature was used as electrolyte to evaluate the performance of the sample, respectively. Linear sweep voltammetry curves at different urea concentrations were recorded at a scanning rate of 1 mV/s. When the urea concentration was 0.3 M, different linear sweep voltammetry characteristic curves were obtained by testing at different sweep speeds (50, 40, 30, 20, 10, and 1 mV/s). Multistep chrono-potentiometry was also performed at different currents and stability tests are also performed to evaluate the performance of the sample.

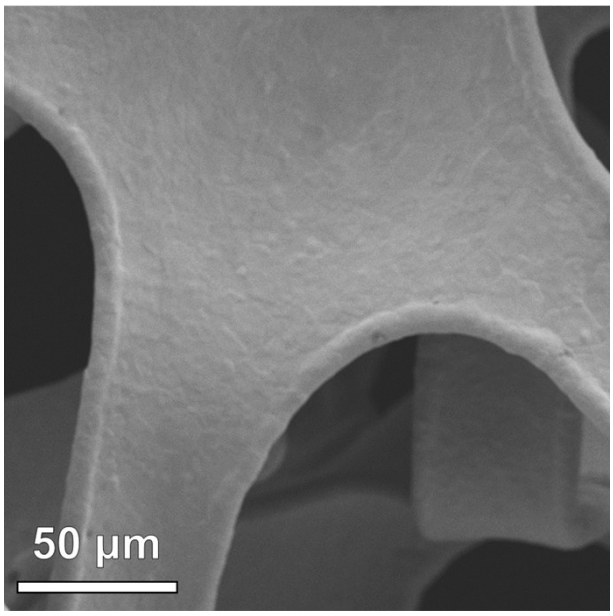

Figure S1. SEM image of Ni foam (NF).

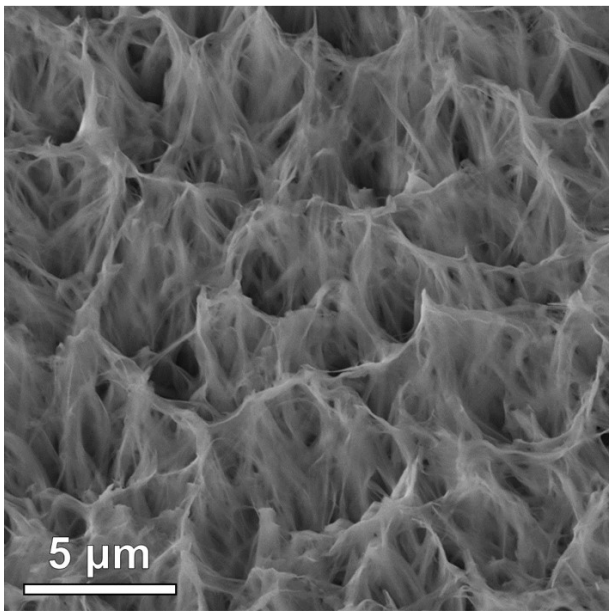

Figure S2. SEM image of the $Ni(SO_4)_{0.3}OH_{1.4}$ precursor.

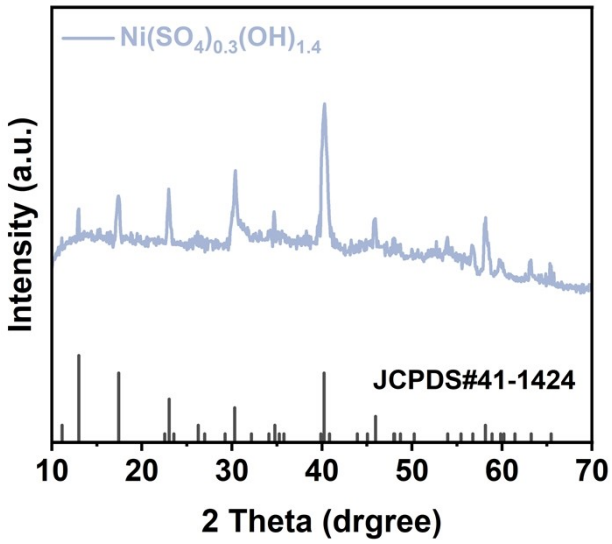

Figure S3. XRD pattern of $Ni(SO_4)_{0.3}OH_{1.4}$ precursor.

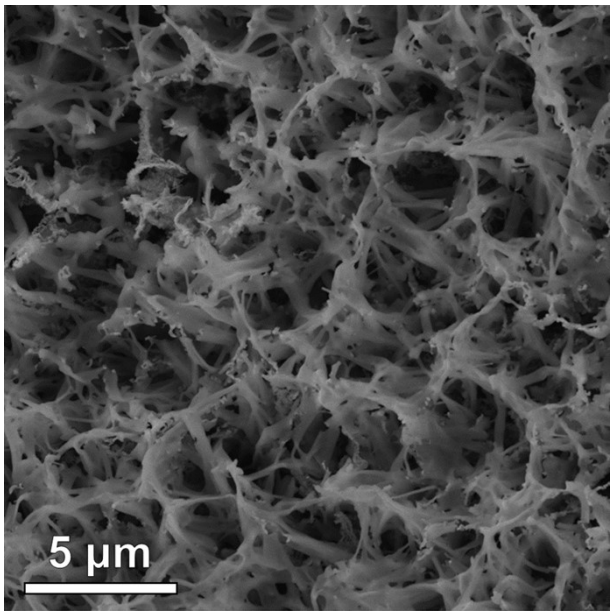

Figure S4. SEM image of the Ni_2P sample.

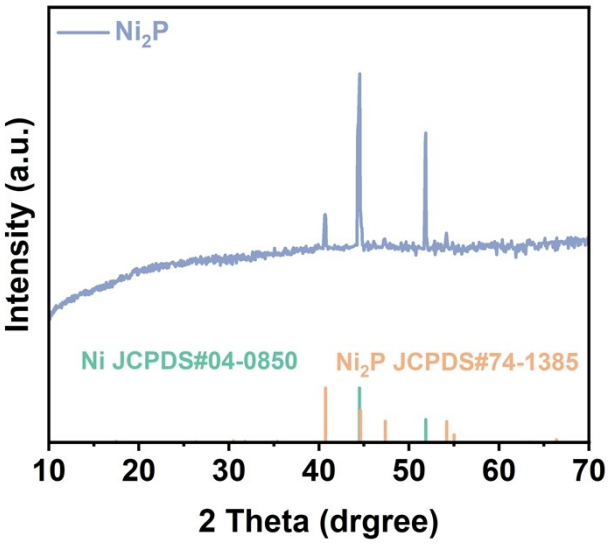

Figure S5. XRD pattern of the Ni_2P samples.

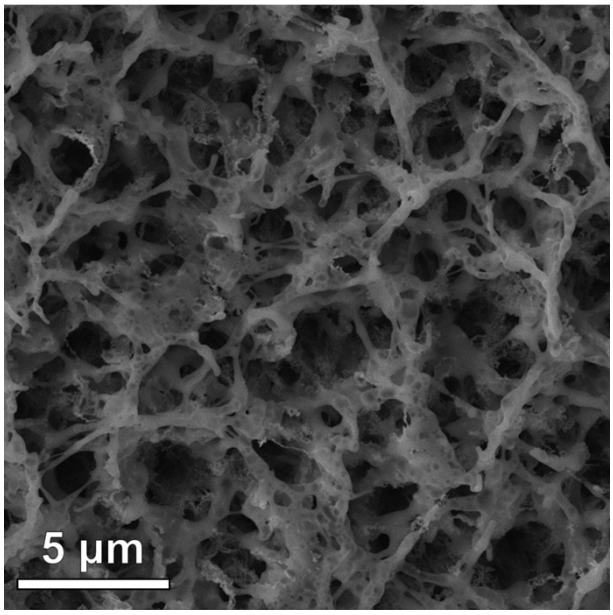

Figure S6. SEM image of the B-Ni_2P sample.

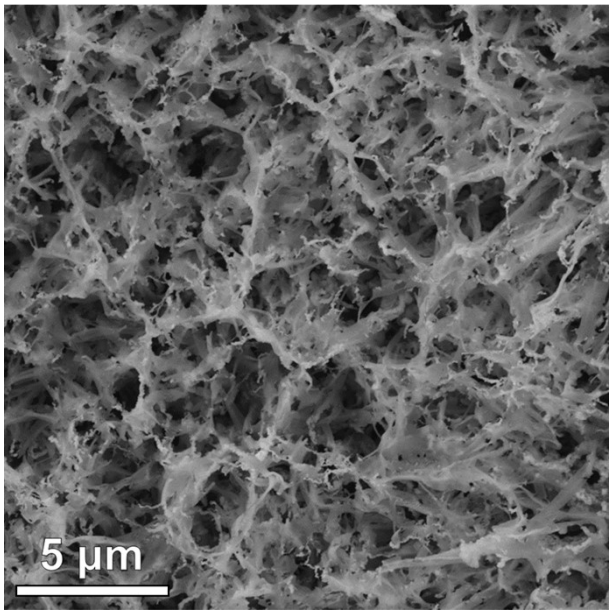

Figure S7. SEM image of the Ni_5P_4 samples.

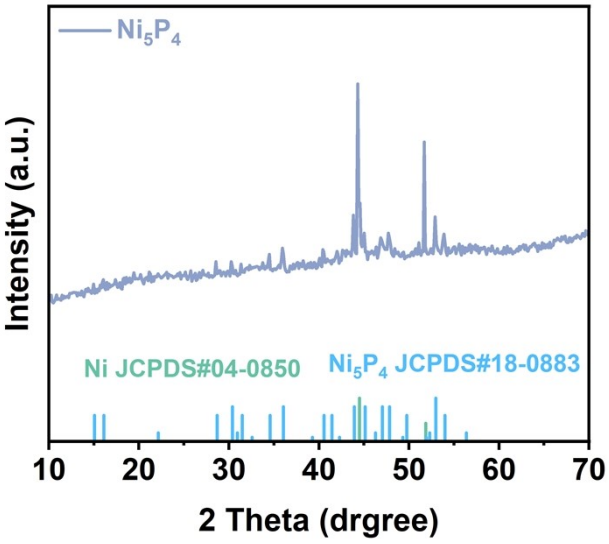

Figure S8. XRD pattern of the Ni_5P_4 samples.

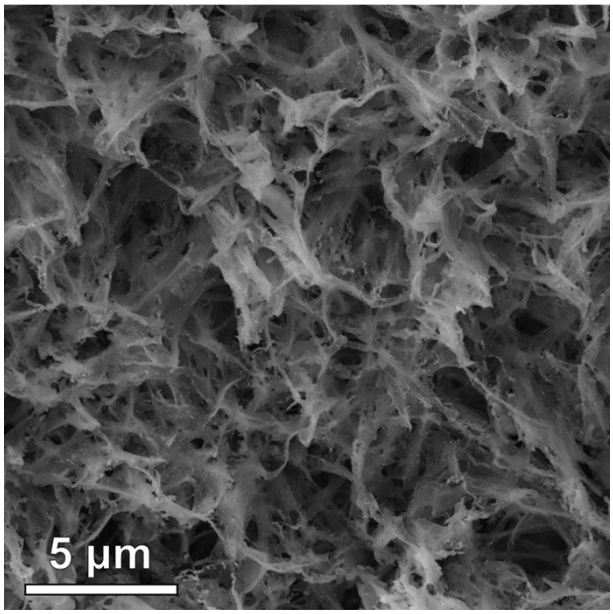

Figure S9. SEM image of the B-Ni_5P_4 samples.

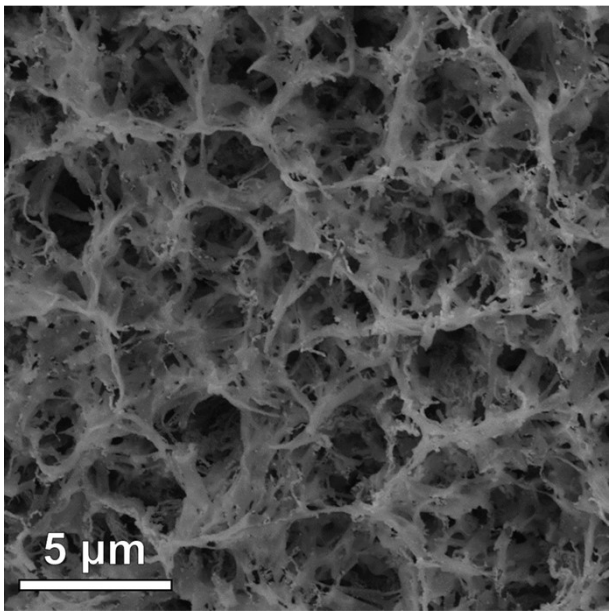

Figure S10. SEM image of the Ni_5P_4/Ni_2P samples.

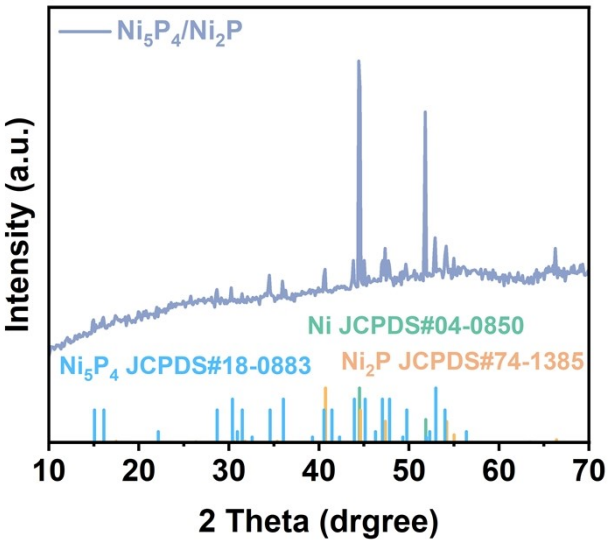

Figure S11. XRD image of the Ni_5P_4/Ni_2P samples.

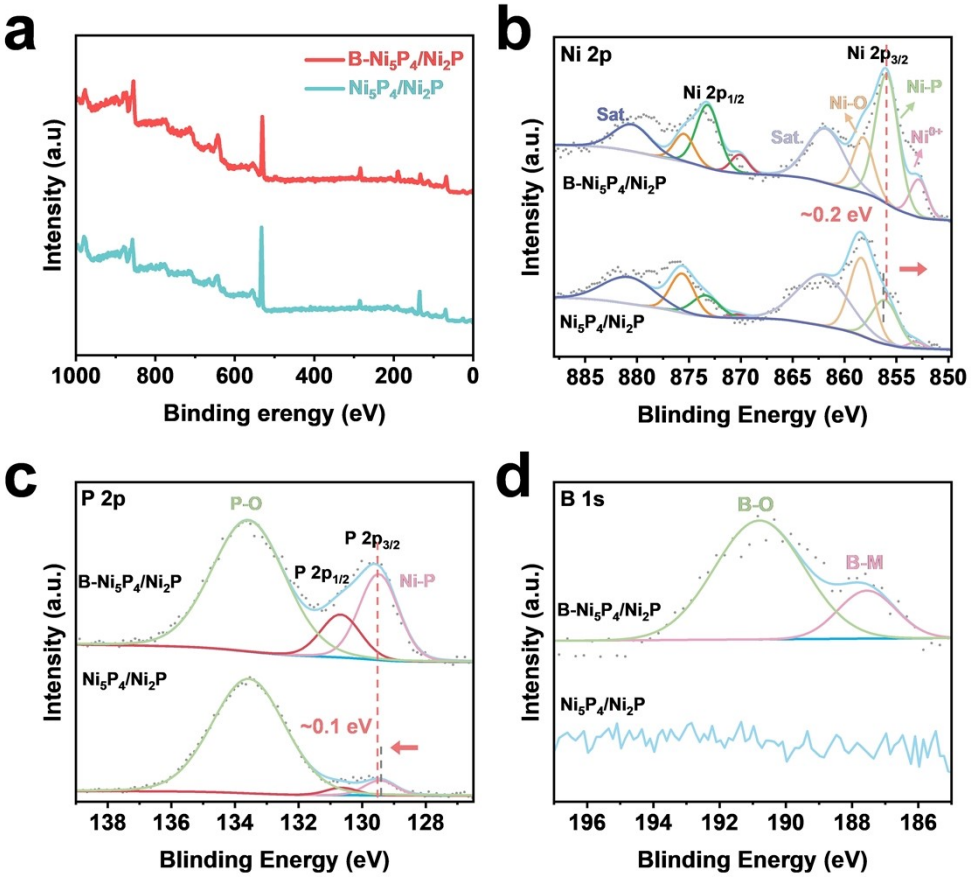

Figure S12. (a) All XPS spectrums of B-Ni_5P_4/Ni_2P and Ni_5P_4/Ni_2P samples. High resolution XPS spectrums of (b) Ni 2p, (c) P 2p, (d) B 1s.

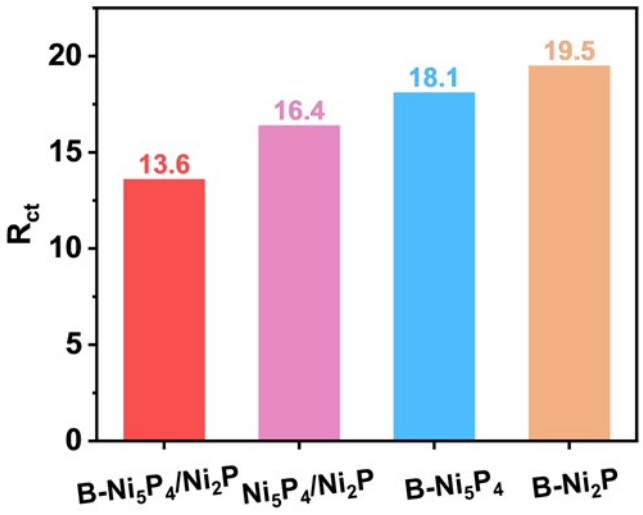

Figure S13. Rct values of these prepared samples. 1,2,3, and 4 stand for B-Ni_5P_4/Ni_2P, Ni_5P_4/Ni_2P, B-Ni_5P_4, and B-Ni_2P samples, respectively.

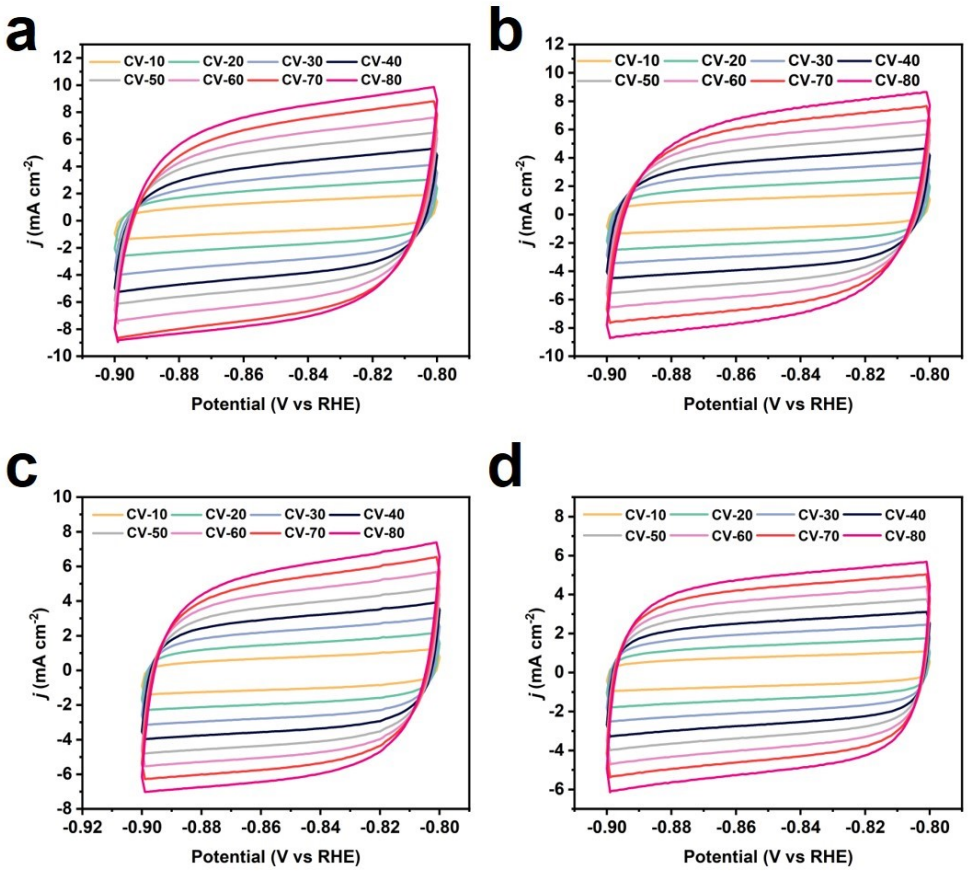

Figure S14. The CV curves of (a) B-Ni_5P_4/Ni_2P, (b) Ni_5P_4/Ni_2P, (c) B-Ni_5P_4, (d) B-Ni_2P tested in 10~80 mV s^{-1} for HER, respectively.

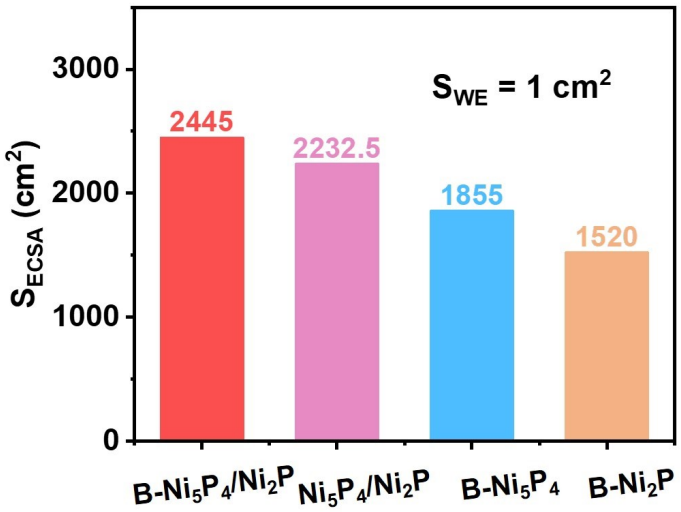

Figure S15. ECSA values of these prepared samples.

Table S1. Comparison of HER performance in 1 M KOH (pH = 14) for the B-Ni_5P_4/Ni_2P with other similar electrocatalysts.

Catalyst	Electrolyte	η (mV) @ 10 mA cm^{-2}	Reference
CoS_2/MoS_2-1	1 M KOH	81	[1]
Co-$Co_{0.85}Se$	1 M KOH	70.79	[2]
NiFe-$LDH_{2.18}$	1 M KOH	72.2	[3]
3D Mo_2C (1:1)	1 M KOH	73.9	[4]
MoS_2/Ni_3S_2	1 M KOH	87	[5]
S-ML-$Nb_4C_3T_x$	1 M KOH	104	[6]
NiO/CeO_2	1 M KOH	78.4	[7]
Mn–N–Co_9S_8 NTs	1 M KOH	107.2	[8]
NiCo-LDH/NCP/NF	1 M KOH	75.6	[9]
B-Ni_5P_4/Ni_2P	**1 M KOH**	**76**	**This work**

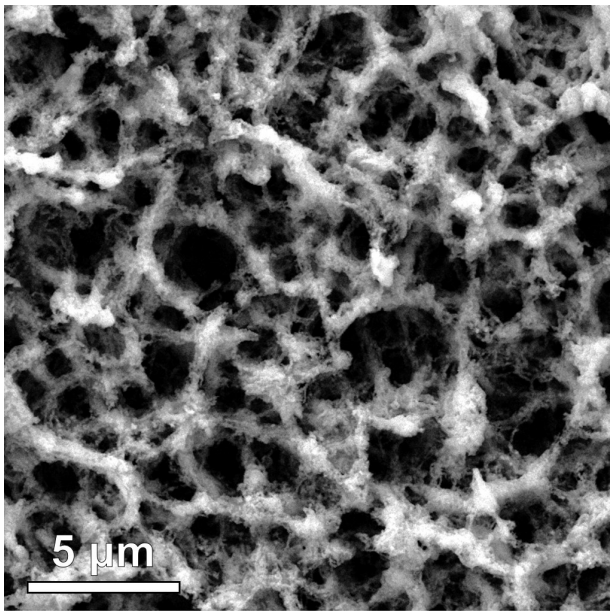

Figure S16. SEM image of B-Ni_5P_4/Ni_2P after HER measurement.

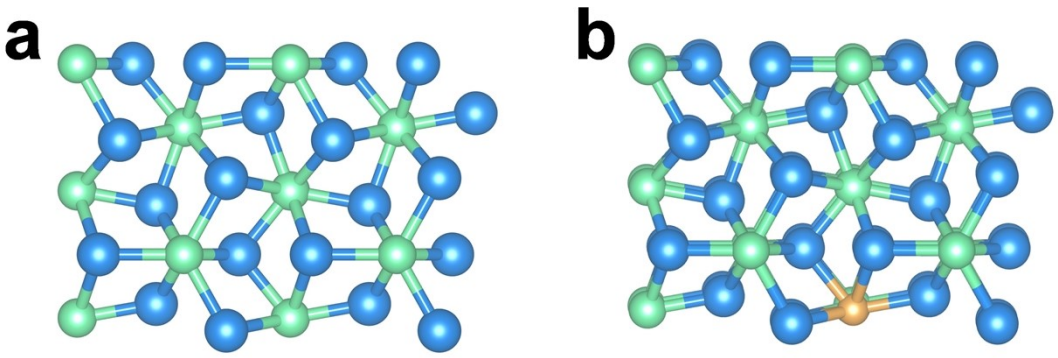

Figure S17. Crystal models of single-phased (a) Ni_2P and (b) B-Ni_2P with (100) surface.

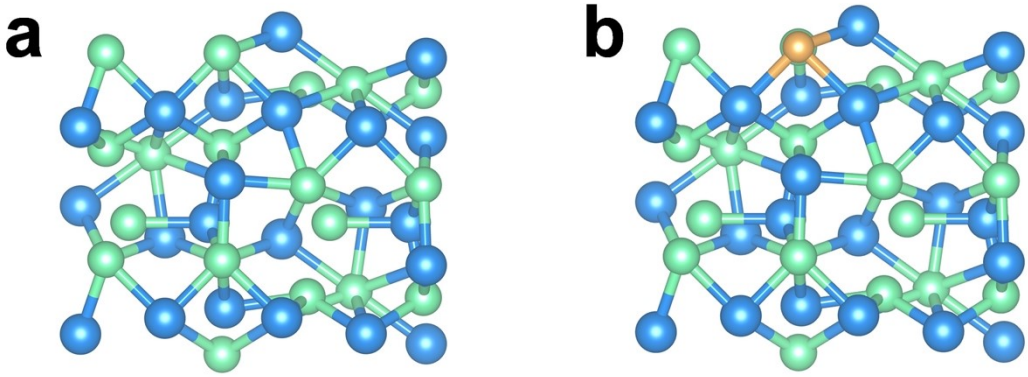

Figure S18. Crystal models of single-phased (a) Ni_5P_4 and (b) B-Ni_5P_4 with (100) surface.

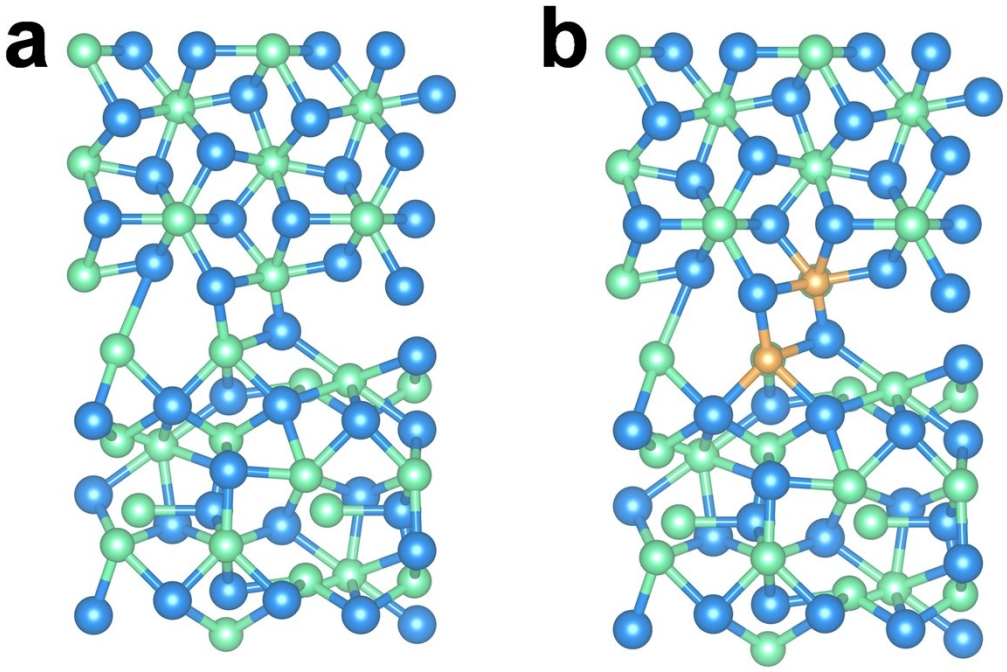

Figure S19. Crystal models of single-phased (a) Ni_5P_4/Ni_2P and (b) B-Ni_5P_4/Ni_2P with (100) surface.

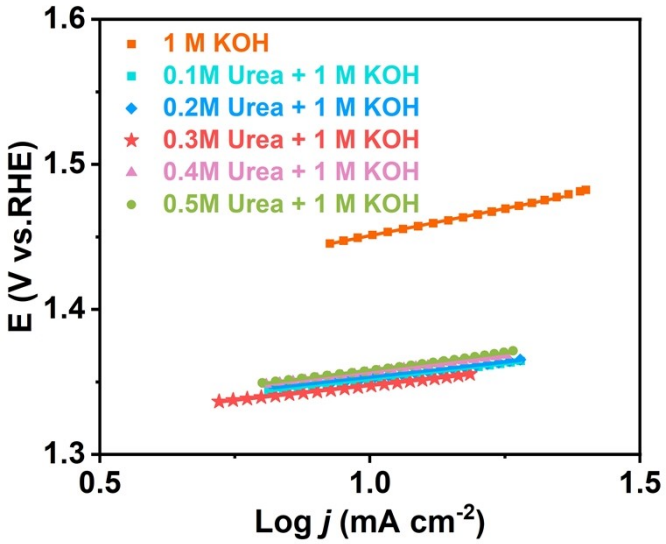

Figure S20. Tafel slopes of the B-Ni_5P_4/Ni_2P sample at different urea concentrations.

Table S2. Comparison of UOR performance in 1 M KOH (pH = 14) for the B-Ni_5P_4/Ni_2P with other similar electrocatalysts.

Catalyst	Electrolyte	E_{10} (V vs. RHE)	Reference
FM@C-1	1 M KOH + 0.33 M Urea	1.45	[10]
NC-FNCP/NF	1 M KOH + 0.5 M Urea	1.37	[11]
Ni@NCDs	1 M KOH + 0.5 M Urea	1.38	[12]
$Ni_{0.05}$/CW	1 M KOH + 0.33 M Urea	1.36	[13]
Ni_3F/Ni_2P	1 M KOH + 0.33 M Urea	1.36	[14]
$NiFeCoS_x@FeNi_3$	1 M KOH + 0.33 M Urea	1.42	[15]
Ni-S-Se/NF	1 M KOH + 0.5 M Urea	1.39	[16]
NiS/MoS_2@CC	1 M KOH + 0.5 M Urea	1.36	[17]
Ni-WO_x	1 M KOH + 0.33 M Urea	1.36	[18]
B-Ni_5P_4/Ni_2P	**1 M KOH + 0.3 M Urea**	**1.35**	**This work**

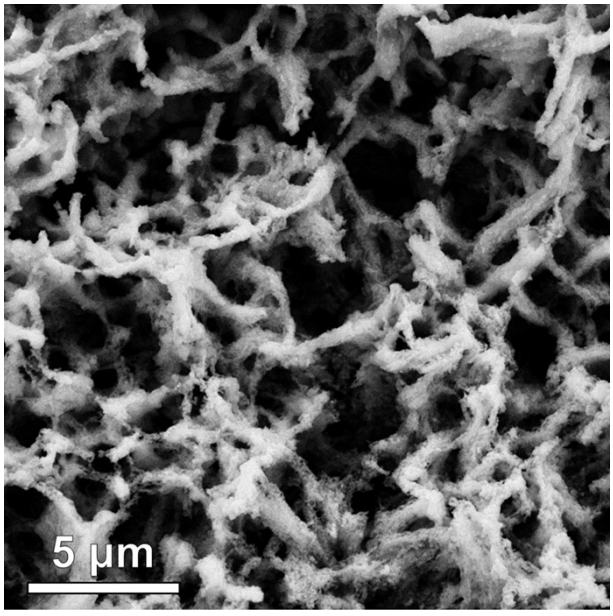

Figure S21. SEM image of B-Ni_5P_4/Ni_2P after UOR measurement.

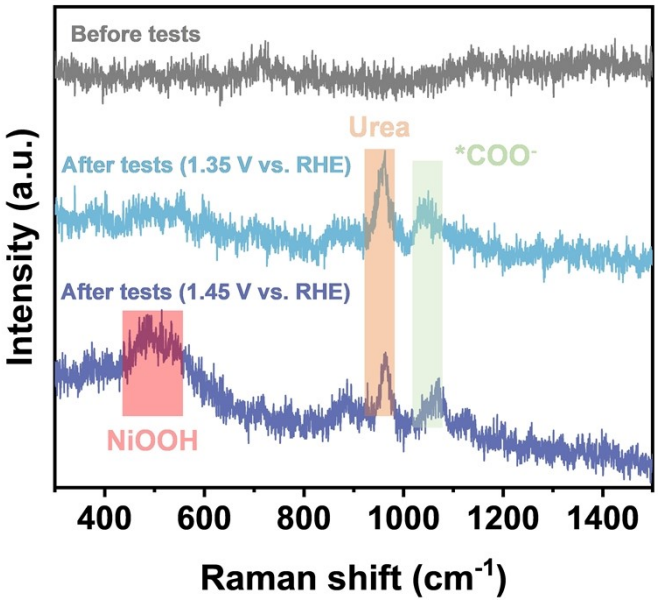

Figure S22. Raman spectrums of before and after UOR stability tests.

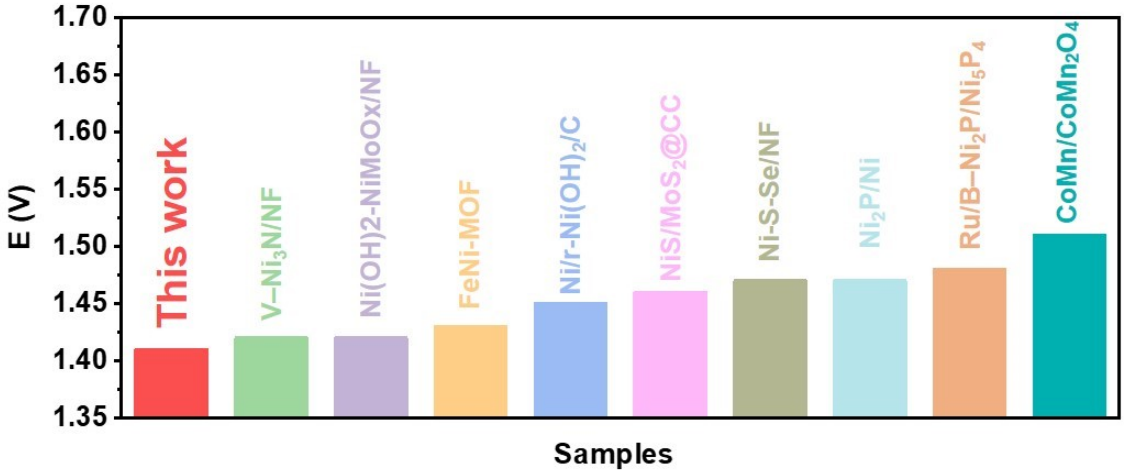

Figure S23. The urea-assisted overall water splitting activity comparison of B-Ni_5P_4/Ni_2P(-) || B-Ni_5P_4/Ni_2P (+) system with other catalysts reported recently**.**

Table S3 Comparison of the urea-assisted water splitting performance of the present catalyst with that of catalysts reported recently in alkaline conditions.

Catalyst	Electrolyte	Cell Voltage (V) @ 10 mA cm^{-2}	Reference
$Ni(OH)_2$-$NiMoO_x$/NF	1 M KOH + 0.33 M urea	1.42	[19]
Ni/r-$Ni(OH)_2$/C	1 M KOH + 0.33 M urea	1.45	[20]
V–Ni_3N/NF	1 M KOH + 0.5 M urea	1.42	[21]
Ru/B–Ni_2P/Ni_5P_4	1 M KOH + 0.5 M urea	1.48	[22]
Ni_2P/Ni	1 M KOH + 0.33 M urea	1.47	[23]
CoMn/$CoMn_2O_4$	1 M KOH + 0.5 M urea	1.51	[24]
NiS/MoS_2@CC	1 M KOH + 0.5 M urea	1.46	[25]
Ni-S-Se/NF	1 M KOH + 0.5 M urea	1.47	[16]
FeNi-MOF	1 M KOH + 0.33 M urea	1.43	[26]
B-Ni_5P_4/Ni_2P || B-Ni_5P_4/Ni_2P	**1 M KOH + 0.3 M urea**	**1.41**	**This work**

References

[1] J. Li, K. Li, Q. Tang, J. Liang, C. Bao, F. Shi, M. Fan, J. Jia, Structure phase engineering strategy through acetic acid coupling to boost hydrogen evolution reaction performance of 2H phase MoS_2 at wide pH range, Fuel, 347 (2023) 128428.

[2] J. Yu, W. Yu, Y. Wang, X. Li, R. Liu, X. Zhang, H. Liu, W. Zhou, Capture and recycling of toxic selenite anions by cobalt-based metal-organic-frameworks for electrocatalytic overall water splitting, Chemical Engineering Journal, 433 (2022) 134553.

[3] X. Li, C. Liu, Z. Fang, L. Xu, C. Lu, W. Hou, Improving the hydrogen evolution performance of self-supported hierarchical NiFe layered double hydroxide via NH3-inducing at room temperature, Journal of Materials Chemistry A, 10 (2022) 20626-20634.

[4] X. Yang, J. Cheng, X. Yang, Y. Xu, W. Sun, J. Zhou, Facet-tunable coral-like Mo_2C catalyst for electrocatalytic hydrogen evolution reaction, Chemical Engineering Journal, 451 (2023) 138977.

[5] L. Zhang, Y. Zheng, J. Wang, Y. Geng, B. Zhang, J. He, J. Xue, T. Frauenheim, M. Li, Ni/Mo Bimetallic-Oxide-Derived Heterointerface-Rich Sulfide Nanosheets with Co-Doping for Efficient Alkaline Hydrogen Evolution by Boosting Volmer Reaction, Small, 17 (2021) 2006730.

[6] F. Wu, C. Xu, X. Yang, L. Yang, S. Yin, S-doped multilayer niobium carbide ($Nb_4C_3T_x$) electrocatalyst for efficient hydrogen evolution in alkaline solutions, International Journal of Hydrogen Energy, 47 (2022) 17233-17240.

[7] X. Hao, X. Zhang, Y. Xu, Y. Zhou, T. Wei, Z. Hu, L. Wu, X. Feng, J. Zhang, Y. Liu, D. Yin, S. Ma, B. Xu, Atomic-scale insights into the interfacial charge transfer in a NiO/CeO_2 heterostructure for electrocatalytic hydrogen evolution, Journal of Colloid and Interface Science, 643 (2023) 282-291.

[8] Y. Xing, D. Li, L. Li, H. Tong, D. Jiang, W. Shi, Accelerating water dissociation kinetic in Co_9S_8 electrocatalyst by mn/N Co-doping toward efficient alkaline hydrogen evolution, International Journal of Hydrogen Energy, 46 (2021) 7989-8001.

[9] L. Zhang, J. Peng, Y. Yuan, W. Zhang, K. Peng, Bifunctional heterostructure NiCo-

layered double hydroxide nanosheets/NiCoP nanotubes/Ni foam for overall water splitting, Applied Surface Science, 557 (2021) 149831.
[10] J. Jana, T. S. K. Sharma, J. S. Chung, W. M. Choi, S. H. Hur, The role of surface carbide/oxide heterojunction in electrocatalytic behavior of 3D-nanonest supported FeiMoj composites, Journal of Alloys and Compounds, 946 (2023) 169395.
[11] J. Zhang, S. Huang, P. Ning, P. Xin, Z. Chen, Q. Wang, K. Uvdal, Z. Hu, Nested hollow architectures of nitrogen-doped carbon-decorated Fe, Co, Ni-based phosphides for boosting water and urea electrolysis, Nano Research, 15 (2021) 1916-1925.
[12] Y. Pan, J. Zhang, Q. Zhang, X. Chen, Q. Wang, C. Li, Z. Liu, Q. Sun, Nickel encapsulated in carbon-dot-derived nanosheets for efficient hydrogen evolution via urea-assisted water electrolysis, Materials Chemistry Frontiers, 7 (2023) 3340-3348.
[13] Y. Liao, S. Deng, Y. Qing, H. Xu, C. Tian, Y. Wu, Hierarchically wood-derived integrated electrode with tunable superhydrophilic/superaerophobic surface for efficient urea electrolysis, Journal of Energy Chemistry, 76 (2023) 566-575.
[14] K. Wang, W. Huang, Q. Cao, Y. Zhao, X. Sun, R. Ding, W. Lin, E. Liu, P. Gao, Engineering NiF_3/Ni_2P heterojunction as efficient electrocatalysts for urea oxidation and splitting, Chemical Engineering Journal, 427 (2022) 130865.
[15] J. Shen, Q. Li, W. Zhang, Z. Cai, L. Cui, X. Liu, J. Liu, Spherical Co_3S_4 grown directly on Ni–Fe sulfides as a porous nanoplate array on $FeNi_3$ foam: a highly efficient and durable bifunctional catalyst for overall water splitting, Journal of Materials Chemistry A, 10 (2022) 5442-5451.
[16] N. Chen, Y.-X. Du, G. Zhang, W.-T. Lu, F.-F. Cao, Amorphous nickel sulfoselenide for efficient electrochemical urea-assisted hydrogen production in alkaline media, Nano Energy, 81 (2021) 105605.
[17] Y. Wang, N. Chen, X. Du, X. Han, X. Zhang, Transition metal atoms M (M = Mn, Fe, Cu, Zn) doped nickel-cobalt sulfides on the Ni foam for efficient oxygen evolution reaction and urea oxidation reaction, Journal of Alloys and Compounds, 893 (2022) 162269.
[18] L. Wang, Y. Zhu, Y. Wen, S. Li, C. Cui, F. Ni, Y. Liu, H. Lin, Y. Li, H. Peng, B. Zhang, Regulating the Local Charge Distribution of Ni Active Sites for the Urea Oxidation Reaction, Angewandte Chemie International Edition, 60 (2021) 10577-

10582.

[19] Z. Dong, F. Lin, Y. Yao, L. Jiao, Crystalline $Ni(OH)_2$/Amorphous $NiMoO_x$ Mixed-Catalyst with Pt-Like Performance for Hydrogen Production, Advanced Energy Materials, 9 (2019) 19002703.

[20] C. Gao, G. Wei, C. Wang, X. Zhou, X. Zhao, Q. Zhao, S. Wang, F. Kong, In situ topologically induced metastable phase Ni/r-$Ni(OH)_2$@C heterostructures with abundant oxygen vacancies as efficient bifunctional electrocatalysts for energy-saving hydrogen production, Journal of Alloys and Compounds, 959 (2023) 17054.

[21] R.-Q. Li, Q. Liu, Y. Zhou, M. Lu, J. Hou, K. Qu, Y. Zhu, O. Fontaine, 3D self-supported porous vanadium-doped nickel nitride nanosheet arrays as efficient bifunctional electrocatalysts for urea electrolysis, Journal of Materials Chemistry A, 9 (2021) 4159-4166.

[22] Y. Wang, Q. Sun, Z. Wang, W. Xiao, Y. Fu, T. Ma, Z. Wu, L. Wang, In situ phase-reconfiguration to synthesize Ru, B co-doped nickel phosphide for energy-efficient hydrogen generation in alkaline electrolytes, Journal of Materials Chemistry A, 10 (2022) 16236-16242.

[23] Q. Li, X. Li, J. Gu, Y. Li, Z. Tian, H. Pang, Porous rod-like Ni_2P/Ni assemblies for enhanced urea electrooxidation, Nano Research, 14 (2020) 1405-1412.

[24] C. Wang, H. Lu, Z. Mao, C. Yan, G. Shen, X. Wang, Bimetal Schottky Heterojunction Boosting Energy-Saving Hydrogen Production from Alkaline Water via Urea Electrocatalysis, Advanced Functional Materials, 30 (2020) 2000556.

[25] C. Gu, G. Zhou, J. Yang, H. Pang, M. Zhang, Q. Zhao, X. Gu, S. Tian, J. Zhang, L. Xu, Y. Tang, NiS/MoS_2 Mott-Schottky heterojunction-induced local charge redistribution for high-efficiency urea-assisted energy-saving hydrogen production, Chemical Engineering Journal, 443 (2022) 136321.

[26] X. Zhang, X. Fang, K. Zhu, W. Yuan, T. Jiang, H. Xue, J. Tian, Fe-doping induced electronic structure reconstruction in Ni-based metal-organic framework for improved energy-saving hydrogen production via urea degradation, Journal of Power Sources, 520 (2022) 230882.